NINETEENTH EUROPEAN ROTORCRAFT FORUM

Paper n° B 1

ELASTIC DEFORMATION OF ROTOR-BLADES DUE TO BVI

by

S. SCHLECHTRIEM, D. NELLESSEN, J. BALLMANN
LEHR- UND FORSCHUNGSGEBIET FÜR MECHANIK
RWTH AACHEN, GERMANY

September 14-16, 1993
CERNOBBIO (Como)
ITALY

ASSOCIAZIONE INDUSTRIE AEROSPAZIALI
ASSOCIAZIONE ITALIANA DI AERONAUTICA ED ASTRONAUTICA

ELASTIC DEFORMATION OF ROTOR-BLADES DUE TO BVI

S. Schlechtriem, D. Nellessen, J. Ballmann
Lehr- und Forschungsgebiet für Mechanik, RWTH Aachen, Germany

1. Abstract

For the prediction of the impact of BVI on the elastic deformation of the rotor-blade the new CFD code SOFIA was developed. SOFIA is based on the well known code INFLEX for the computation of unsteady, transonic flows about airfoils and the new method ODISA for the calculation of the structural deformations. The major aim of the investigation is the prediction of the impact of BVI loads on the rotor-blade structure and the analysis of appropriate active control systems. With a view to the design of Higher Harmonic Pitch Control Systems or Individual Blade Control Systems the knowledge of the time history of the blade's deformation is indispensable. Therefore emphasis was put on the correct treatment of the propagation of stress waves and the related deformations during the development of ODISA.

2. List of Symbols

FLOW PART:

c	chord length
C_L	lift coefficient
C_m	moment coefficient
e	total specific energy
$\mathbf{E}$, $\mathbf{F}$, $\mathbf{G}$	fluxes
$\mathbf{I}$	unit matrix
J	Jacobian
M	Mach number
p	pressure
$\mathbf{v}$	flow velocity
Φ	matrix of flow variables
Λ	velocity of the grid (components $\dot{x}$, $\dot{y}$, $\dot{z}$)
ρ	density
$\Delta\tau$	time increment
Γ	circulation
ψ	rotor azimuthal angle
ω	relaxation parameter

Indices:

∞	infinity
w	vortex position
i, j, k	space directions
μ, γ	iteration indices

Coordinate System:

x, y, z, t	inertial reference system (Euler coordinates),time
ξ, η, ζ, τ	curvilinear coordinates ,time

Letters in bold-face type indicate vectors or matrices. The summation convention for double greek indices is used.

STRUCTURAL PART:

$\mathbf{a}$	acceleration
EA	tension stiffness
$\mathbf{EI}$	bending stiffness matrix
$\mathbf{GA}$	shear stiffness matrix
GI_T	torsional stiffness
f	Riemann invariant
$\mathbf{M}$	moment
N	normal force
$\mathbf{q}$	transverse load per unit length
$\mathbf{Q}$	shear force
$\mathbf{u}$	displacement
φ	rotation by deformation
γ	shear angle
ρI	rotatory inertia
ρA	mass per length
$\Delta\tau$	time increment
ω	angular velocity
Ω	tensor of angular velocities

Indices:

A	input kinematics (RA main rotor axis, cA cyclic pitch variation)
B	bending, bending centre
C	cross-sectional centre of gravity
D	shear centre
CD,CB	distances between centres
T	torsion

Coordinate Systems:

$O'x'$	inertial reference frame, e'_i
Ox	rotating reference frame (Ω_A), e_i
$O\xi$	material reference system, e_{Si}

3. Introduction

The interactions of the rotor-blade with the tip vortices of the preceding blades (BVI) can cause a significant increase in noise and vibration. Especially during descent flight conditions at advance ratios of 0.1 ÷ 0.2 BVI is the major source of noise and has a tremendous effect on vibratory airloads because of the small vertical distance between the tip vortex of the previous blade and the rotor-blade itself. In the past many efforts to enlighten the BVI mechanism have been undertaken. Experiments were carried out by Meier et al /1/, Caradonna et al /2/, Bershader et al /3/, and Galbraith et al /4/ . Numerical methods were applied by Caradonna et al /5/, McCroskey et al /6/ and Ballmann et al /7/, /8/. These investigations show that the fundamental BVI phenomenon is understood fairly well.

During the last two decades active control systems like Higher Harmonic Pitch Control /9/ and Individual Blade Control /10/ have been developed. The control movements of the active control devices are additional pitch motions which influence the angle of attack in an appropriate way to minimize vibration and to reduce BVI noise. As experiments with rotor-blade models which fulfill all the required similarity laws are almost impossible, windtunnel tests are usually only performed with very stiff models of the actual blade. Aeroelastic effects are therefore neglected during these investigations. But because of the torsional and bending flexibility of realistic blades the rotor-blade deforms during the blade-vortex interaction. Of course this deformation has a feedback on the airloads and the pressure distribution. Especially the "compressibility" wave and the "transonic" wave which are of major importance concerning BVI noise are changed significantly. In this connection the additional control movements from the active control devices need to be mentioned. As the blade is flexible a time lag between the control movement at the blade's root and the desired change of the angle of attack at the blade's tip to reduce BVI noise occurs.

The present paper describes the new method SOFIA (Solid-Fluid-Interaction) which was developed to model and analyze aeroelastic phenomena. A brief description of the two modules - INFLEX for the flow analysis and ODISA (One-Dimensional Structural Analysis) for the structural analysis - that are required to accomplish BVI computations for rigid and especially elastic rotor-blades is provided. The well-known code INFLEX was developed by Eberle and Brenneis /11/. A comprehensive evaluation was carried out based on the Two- and Three-dimensional AGARD Standard-Configurations /12/. The computations shown here represent the first efforts to compute aeroelastic phenomena during BVI. They demonstrate the feasibility of SOFIA to take blade motions due to cyclic pitch variations, active control and blade deformation into account.

4. Solution Procedures

SOFIA is a code to model and analyze aeroelastic phenomena. A schematic of the SOFIA solution procedure is shown in Figure 1. It can be seen that during each time step several different subiterations concerning the flow analysis part (INFLEX) and the structural analysis part (ODISA) have to be performed. Once the flow solution at iteration level γ (see Chapter 4.1) is obtained, the airloads are input for the structural loop. Due to the unsteady airloads the blade deforms. The deformation is defined by the torsional angle, two bending angles and three displacements if the structure is assumed to be one-dimensional. As a consequence the deformation velocities of the

blade have to be taken into account in addition to the prescribed blade motions (cyclic pitch, rotation of the main rotor-axis and active control).

4.1 Flow Analysis

The major task during the investigation of BVI is the prediction of the unsteady flow phenomena on the advancing side of the rotor. The blade-vortex interactions are usually most intense at azimuthal angles between $\Psi = 20^\circ$ and 70° degrees. At $\Psi = 90^\circ$ the relative flow velocity reaches its maximum and supersonic pockets occur at the blade's tip (see Figure 2). Due to the cyclic pitch variation the angle of attack on the advancing side is kept small to balance the lift distribution. In contrast to the retreating side of the rotor where separation occurs the flow on the advancing side is attached and the assumption of an inviscid flow is justified as long as the tip vortices of the preceding blades do not collide with the blade. In the present investigation a clockwise rotating vortex passing the underside of the rotor is considered (see Figure 3). For the computation of the unsteady, compressible, inviscid flow about the rotor-blade the well known code INFLEX based on the Euler equations is used.

With respect to an inertial reference system and for time dependent boundary conditions, the balance equations of mass (1), momentum (2) and energy (3) are:

$$\frac{d}{dt}\int_{V(t)} \rho dV + \int_{\partial V(t)} \rho (v - \Lambda)\cdot \mathbf{n} dS = 0 \quad , \tag{1}$$

$$\frac{d}{dt}\int_{V(t)} \rho v dV + \int_{\partial V(t)} v\,[\rho (v - \Lambda)\cdot \mathbf{n}] dS = -\int_{\partial V(t)} p\mathbf{n} dS \quad , \tag{2}$$

$$\frac{d}{dt}\int_{V(t)} e dV + \int_{\partial V(t)} e\,(v - \Lambda)\cdot \mathbf{n} dS = -\int_{\partial V(t)} p\,(v\cdot \mathbf{n}) dS \quad . \tag{3}$$

The velocity of the grid is denoted Λ.

Applying Gauß' theorem, the surface integrals in the balance equations can be transformed into volume integrals. Assuming that the flow variables are constant throughout a small finite volume, a strong conservation form of the partial differential equations (PDE's) is obtained from the transformation into the space of coordinates used in the numerical calculation:

$$\frac{\partial \Phi}{\partial \tau} + \frac{\partial \mathbf{E}}{\partial \xi} + \frac{\partial \mathbf{G}}{\partial \zeta} + \frac{\partial \mathbf{F}}{\partial \eta} = 0 \quad , \qquad \Phi^T = (\rho,\ \rho u,\ \rho v,\ \rho w,\ e)\, J \quad , \tag{4}$$

with J, the Jacobian of the transformation, and the fluxes

$$E = J\,(\tilde{E}\xi_{,x} + \tilde{F}\xi_{,y} + \tilde{G}\xi_{,z}) \quad , \qquad F = J\,(\tilde{E}\eta_{,x} + \tilde{F}\eta_{,y} + \tilde{G}\eta_{,z}) \quad ,$$

$$\mathbf{G} = J\,(\tilde{E}\zeta_{,x} + \tilde{F}\zeta_{,y} + \tilde{G}\zeta_{,z}) \tag{5}$$

where

$$\tilde{E} = \begin{bmatrix} \rho(u - \dot{x}) \\ \rho u\,(u - \dot{x}) + p \\ \rho v\,(u - \dot{x}) \\ \rho w\,(u - \dot{x}) \\ e\,(u - \dot{x}) + pu \end{bmatrix} \quad \tilde{F} = \begin{bmatrix} \rho\,(v - \dot{y}) \\ \rho u\,(v - \dot{y}) \\ \rho v\,(v - \dot{y}) + p \\ \rho w\,(v - \dot{y}) \\ e\,(v - \dot{y}) + pv \end{bmatrix} \quad \tilde{G} = \begin{bmatrix} \rho(w - \dot{z}) \\ \rho u\,(w - \dot{z}) \\ \rho v\,(w - \dot{z}) \\ \rho w(w - \dot{z}) + p \\ e\,(w - \dot{z}) + pw \end{bmatrix} .$$

The corresponding first order time-discretized implicit equations

$$\frac{\Phi^{n+1} - \Phi^n}{\Delta\tau} + \frac{\partial E^{n+1}}{\partial\xi} + \frac{\partial F^{n+1}}{\partial\eta} + \frac{\partial G^{n+1}}{\partial\zeta} = 0 \qquad (6)$$

are nonlinear and therefore solved iteratively by constructing a sequence of approximations, such that

$$\lim_{\mu\to\infty} \Phi^{\mu} = \Phi^{n+1} \quad . \qquad (7)$$

Linearizing the fluxes in (6) the Newton-method reads:

$$\frac{\Delta\Phi^{\mu+1}}{\Delta\tau} + \frac{\partial}{\partial\xi}(\mathcal{A}^{\mu}\,\Delta\,\Phi^{\mu+1}) + \frac{\partial}{\partial\eta}(\mathcal{B}^{\mu}\,\Delta\,\Phi^{\mu+1}) + \frac{\partial}{\partial\zeta}(\mathcal{C}^{\mu}\,\Delta\,\Phi^{\mu+1}) \qquad (8)$$

$$= -\left(\frac{\Phi^{\mu} - \Phi^n}{\Delta\tau} + \frac{\partial E^{\mu}}{\partial\xi} + \frac{\partial F^{\mu}}{\partial\eta} + \frac{\partial G^{\mu}}{\partial\zeta}\right) \quad , \qquad \Delta\Phi^{\mu+1} = \Phi^{\mu+1} - \Phi^{\mu} \quad ,$$

with the Jacobians $\mathcal{A}$, $\mathcal{B}$, $\mathcal{C}$ of the fluxes. The flux differences $E_{,\xi}$, $F_{,\eta}$ and $G_{,\zeta}$, appearing on the right hand side ($\mathcal{RHS}$), are calculated by means of a characteristic extrapolation with third order accuracy in domains with smooth solution behaviour and first order accuracy in the proximity of shocks /13/. This method is based on a dimensional splitting yielding locally one-dimensional Riemann problems. By using a characteristic variables splitting technique, the flux differences appearing on the left hand side ($\mathcal{LHS}$), are divided up into a part which is related to the positive eigenvalue and into another part that is related to the negative eigenvalues. An upwind scheme of first order is employed.

Since the direct solution of the Newton iteration is very time-consuming, a relaxation technique is used /14/: The off-diagonal elements $\mathcal{ODIAG}$ of the left hand side coefficient matrix are shifted to the right hand side. Thus, an equation of the form

$$\left(\frac{I}{\Delta\tau} + \mathcal{DIAG}^{\mu}_{i,j,k}\right)\Delta\Phi^{(\mu+1)^{\nu}}_{i,j,k} = \omega\cdot\mathcal{RHS}^{\mu}_{i,j,h} + \mathcal{ODIAG}_{i,j,k} \qquad (9)$$

is obtained. Here, ν is the point Gauß-Seidel iteration index. During a Gauss-Seidel iteration, $\mathcal{RHS}$ and $\mathcal{DIAG}$ remain at the μ-level. Applying a so-called checkerboard scheme, $\mathcal{ODIAG}$ is calculated partly from the previous and partly from the present values of $\Delta\Phi$. Thus, a compromise between a high degree of vectorization (by using the previous values of $\Delta\Phi$) and a high rate of convergence (by using the present values of $\Delta\Phi$) has been made. The underrelaxation factor ω compensates the error that arises from the different spatial order of accuracy on the $\mathcal{RHS}$ and $\mathcal{LHS}$.

An H-type grid with a high resolution in the proximity of the convecting vortex was chosen. It rotates about the helicopter's main rotor axis. Additional motion caused by elastic wing deformation and cyclic pitch variation is taken into account by moving the inner boundary of the grid which represents the blade's surface while the outer boundary of the rotor-blade fixed grid remains unchanged. Therefore, the grid needs to be renewed at each time step. This is done iteratively by solving an appropriate Poisson equation /15/. Since each new grid deviates only slightly from the grid at the preceding time step, only few iterations are necessary.

4.2 Structural Analysis

During the development of the new method ODISA emphasis was put on the correct treatment of the propagation of stress waves and the related deformations /16/. At the first glance this kind of structural model seems to be unusual compared to other methods which mainly originate from Euler-Bernoulli-beam theory and use modal analysis for the description of the unsteady deformations. However, modal analysis is based on the assumption that the wave propagation speed of tranverse, torsional and longitudinal waves is large compared to the ratio of the rotor-blade span and the relevant time scales. But in case of rotor-blades torsional stress waves propagate at a slow speed so that the time period to establish a well developed oscillation is longer than the physical relevant time (e.g. duration of BVI). Therefore another model with a different mathematical background is needed:

It turns out that rotor-blades have a torsional wave speed of only about 500 m/s (comparison: speed of the torsional wave in steel is approximately 3000 m/s). During a parallel blade-vortex-interaction which takes place within 10 degrees azimuth (5 milliseconds) a torsional wave can travel only about 2.5 m (less than the rotor-blade's span). Therefore it is necessary to simulate the wave propagation process correctly in order to estimate the dynamical behaviour of the blade.

Due to the 6 DOF (rotation, translation) of a beam's cross section, the governing equations are the following:

Equation of momentum

$$\rho A \mathbf{a}'_C = \frac{\partial}{\partial \xi_1}(\mathbf{N} + \mathbf{Q}) + \mathbf{q} \quad , \tag{10}$$

where $\mathbf{a}'_C$ is the acceleration of the centre of gravity of a material cross-section

$$\mathbf{a}'_C \doteq \mathbf{a}'_O + \mathbf{a}_C + \xi_{C\alpha}\,\dot{\boldsymbol{\omega}} \wedge \mathbf{e}_\alpha + \xi_1\,\boldsymbol{\omega}_A \wedge (\boldsymbol{\omega}_A \wedge \mathbf{e}_1) \quad , \qquad \alpha = 2, 3$$

with

$$\boldsymbol{\omega} = \dot{\boldsymbol{\varphi}} + \boldsymbol{\omega}_A \quad , \qquad \boldsymbol{\omega}_A = \boldsymbol{\omega}_{RA} + \boldsymbol{\omega}_{cA} \quad .$$

Equation of moment of momentum for $\dot{\boldsymbol{\omega}}_{RA} = 0$

$$\begin{aligned} \rho I_C (\ddot{\boldsymbol{\varphi}} + \dot{\boldsymbol{\omega}}_{cA}) \doteq\ & \frac{\partial}{\partial \xi_1}(\mathbf{M}_T + \mathbf{M}_B) + \mathbf{m} - \boldsymbol{\omega}_A \wedge [\rho I_C (\boldsymbol{\omega}_A + \dot{\boldsymbol{\varphi}})] \\ & + \frac{\partial}{\partial \xi_1}(\xi_{CD\alpha}\,\mathbf{e}_{s\alpha} \wedge \mathbf{Q} + \xi_{CB\alpha}\,\mathbf{e}_{s\alpha} \wedge \mathbf{N}) \\ & + \left[\mathbf{e}_1 + \frac{\partial}{\partial \xi_1}(\xi_{CB\alpha}\,\mathbf{e}_{s\alpha} + \mathbf{u})\right] \wedge (\mathbf{N} + \mathbf{Q}) \quad , \qquad \alpha = 2, 3 \quad . \end{aligned} \tag{11}$$

The kinematical approximation for the deformation part of the blade motion is given by

$$\mathbf{u}_D = \mathbf{u} + \boldsymbol{\varphi} \wedge \xi_{D\alpha}\,\mathbf{e}_\alpha \quad ; \qquad \alpha = 2, 3$$

$$\gamma_2 = u_{2,\xi_1} - (\varphi_T \xi_{D3})_{,\xi_1} - \varphi_{B3} \quad ; \quad \gamma_3 = u_{3,\xi_1} - (\varphi_T \xi_{D2})_{,\xi_1} - \varphi_{B2} \quad . \tag{12}$$

Constitutive equations within the scope of Timoshenko's approximation are

$$\mathbf{N} = EA\,u_{1,\xi_1}\mathbf{e}_1, \quad \mathbf{Q} = GA\kappa\gamma, \quad \mathbf{M}_T = GI_T \varphi_{T,\xi_1}\mathbf{e}_1, \quad \mathbf{M}_B = EI\,\varphi_{B\alpha,\xi_1}\mathbf{e}_1 \quad , \quad \alpha = 2, 3 \quad . \tag{13}$$

Equations (10) to (13) can be transformed into a system of 12 linear, first order, partiell differential equations which is of hyperbolic type. Due to Timoshenko and Flügge the effects of shear flexibility and rotatory inertia are included. This is important if phenomena where short wavelengths occur (e.g. BVI, active control) are considered. Using a matrix notation the system of differential equations reads

$$\tilde{\mathcal{A}}\tilde{f}_{,\tau} - \tilde{\mathcal{B}}\tilde{f}_{,\xi 1} = \tilde{C}\tilde{f} + \tilde{d} \quad ,$$

$$\tilde{f}^T = (v_1, v_2, v_3, \omega_T, \omega_{B2}, \omega_{B3}, N, Q_2, Q_3, M_T, M_{B2}, M_{B3})$$

$$= \left(\tilde{f}^T_{VEL}, \tilde{f}^T_{LOAD}\right) \quad . \qquad (14)$$

The canonical form of the linear, hyperbolic set of differential equations /20/ is given by

$$f_{,\tau} - \mathcal{B} f_{,\xi 1} = Cf + d \quad , \qquad (15)$$

with the definitions

$$\mathcal{B} := \tilde{\Lambda} = \tilde{\Gamma}^{(-1)}\, \tilde{\mathcal{A}}^{(-1)}\, \tilde{\mathcal{B}}\, \tilde{\Gamma} \quad ,$$

$$C := \tilde{\Gamma}^{(-1)}\, \tilde{\mathcal{A}}^{(-1)}\, \tilde{C}\tilde{\Gamma} - \tilde{\Lambda}\, \tilde{\Gamma}^{(-1)}_{,\xi 1}\, \tilde{\Gamma} + \tilde{\Gamma}^{(-1)}_{,\tau}\, \tilde{\Gamma} \quad , \qquad d := \tilde{\Gamma}^{(-1)} \tilde{\mathcal{A}}^{(-1)} \tilde{d} \quad . \qquad (16)$$

$\tilde{f} = \tilde{\Gamma}^{(-1)}\, \tilde{f}$ are the Riemann invariants. The real eigenvalues of $\tilde{\mathcal{A}}^{(-1)}\, \tilde{\mathcal{B}}$ form the main diagonal of the spectral matrix $\tilde{\Lambda}$ and the eigenvectors of $\tilde{\mathcal{A}}^{(-1)}\, \tilde{\mathcal{B}}$ are the columns of the modal matrix $\tilde{\Gamma}$. The time derivative of the Riemann invariants along their associated characteristic (index (j)) is defined by

$$\frac{D^{(j)} f_j}{D\tau} = f_{j,\tau} - \lambda_j f_{j,\xi_1} \quad , \qquad j = 1, 2, \ldots, 12 \qquad (17)$$

and the characteristic directions are found using

$$\frac{D^{(j)} \xi_1}{D\tau} = -\lambda_j \quad , \qquad j = 1, 2, \ldots, 12 \qquad (18)$$

Along the characteristic directions the so-called compatibility relations hold:

$$\frac{D^{(j)} f_j}{D\tau} = \sum_{k=1}^{12} C_{jk} f_k + d_j \quad , \qquad j = 1, 2, \ldots, 12 \qquad (19)$$

For the numerical integration of the compatibility relations the method of Heun is used (*indicates values at the new time level, o defines the values at the old time level of the j-th characteristic)

$$f_j^{(*)} = f_j^{(o)} + \frac{1}{2}\Delta\tau \left\{ \sum_{k=1}^{12} \left[(C_{jk} f_k)^{(*)} + (C_{jk} f_k)^{(o)} \right] + d_j^{(*)} + d_j^{(o)} \right\}$$

in matrix notation:

$$\left(1 - \frac{1}{2}\Delta\tau C^{(*)}\right) f^{(*)} = f^{(o)} + \frac{1}{2}\Delta\tau \left\{ (Cf)^{(o)} + d^{(*)} + d^{(o)} \right\} \qquad (20)$$

The application of a series expansion

$$\left(1 - \frac{1}{2}\Delta\tau C^{(*)}\right)^{-1} = 1 + \frac{1}{2}\Delta\tau C^{(*)} + \frac{1}{4}\Delta\tau^2 C^{(*)} C^{(*)} + O(\Delta\tau^3) \qquad (21)$$

leads to the finite difference equation for interior grid points

$$f^{(*)} = f^{(o)} + \frac{1}{2}\Delta\tau\left(I + \frac{1}{2}\Delta\tau C^{(*)}\right)\left[C^{(*)} f^{(o)} + (Cf)^{(o)} + d^{(*)} + d^{(o)}\right] \quad . \qquad (22)$$

Each wave is traced in its own grid so that numerical dissipation usually caused by interpolation errors is minimized. At the left and right boundaries of the one-dimensional structure six boundary conditions have to be fulfilled. In case of a hingeless rotor-blade all the kinematic variables like torsional angle, bending angles, shear angles and displacements are specified at the blade's root. At the tip of the blade the dynamic variables (moments, forces) are given.

4.3 Aeroelastic Analysis

For a fully coupled analysis of the flow part and the structural part the following equations have to be solved simultaneously:

1. Step Computation of the actual structural deformation

$$\tilde{\mathcal{A}}\tilde{f}_{,\tau} - \tilde{\mathcal{B}}\tilde{f}_{,\xi 1} = \tilde{C}\tilde{f} + \tilde{d} \quad \Rightarrow \quad u_{DEF} = u_O + \int \tilde{f}_{VEL} D\tau \qquad (23)$$

2. Step Computation of the actual flow and calculation of the airloads

$$\Phi_{,\tau} + E_{,\xi} + F_{,\eta} + G_{,\zeta} = 0 \quad \Rightarrow \quad \Phi^{n+1} \quad \Rightarrow \quad \tilde{d} \qquad (24)$$

The schematic (see Figure 1) shows an additional subiteration within one time step. During this iteration the airloads $\tilde{d}$ are updated by averaging between the old and the new time level

$$\tilde{d} = a \cdot \tilde{d}^{n} + (1 - a)\,\tilde{d}^{n+1} \quad . \qquad (25)$$

This process is repeated until the relative changes in the solution disappear.

5. Results

Various unsteady test cases have been calculated /12/, /17/ to evaluate SOFIA. The computation of the Standard AGARD-Test-Cases for pitching and plunging airfoils/ wings with INFLEX shows good agreement with experiments and results from other authors. As mentioned above the parallel blade-vortex-interaction has been investigated by many researchers and a lot of computational /8/ and experimental results /4/ are available to compare with. Here a test case with freestream Mach number M_∞ = 0.73, vertical distance between vortex and airfoil at infinity $y_{w\infty}$=-0.26, circulation of the vortex Γ = 0.4 is considered. The computation is initialized by computing a steady state solution and introducing the vortex 4 chord lenghts in front of the airfoil's leading edge. A Lamb type model is used to describe the initial structure of the vortex. Figure 4 shows the feasibility of SOFIA to predict the relevant flow phenomena

like "compressibility" and "transonic" waves. The unsteady lift distribution is given in Figure 5. A comparison with other methods shows good agreement.

Based on these preliminary computations to evaluate SOFIA, computational studies taking the elasticity of the rotor-blade into account have been performed. In case elastic deformations occur the rotor-blade deforms. Figur 6 shows the results for a test case with two degrees of freedom (pitch: $\overline{\omega}_1 = 1$, plunge: $\overline{\omega}_2 = 1.2$). Depending on the distance between the shear centre and the centre of gravity the time histories change significantly. Obviously energy is transferred from plunge to pitch. The comparison of the lift and moment distribution with a rigid blade solution shows that the elastic deformations have a tremendous effect on the airloads.

An analysis of a complete three-dimensional interaction of a vortex with an elastic rotor-blade (Figure 7) was performed. The rotor-blade is linearly twisted and has an aspect ratio of 10. The grid consists of 80 points in azimuthal direction, 40 points in axial direction and 40 points in radial direction. In opposite to a full analysis of a helicopter rotor in forward flight where a fully converged periodic solution of the flowfield is calculated /18/, /19/ here only one BVI phenomenon is numerically simulated. Figure 8 shows the angle of attack as a function of time. In case of a rigid-rotor-blade the angle of attack remains constant. In Figures 9 and 10 a comparison of the airloads for an elastic and a rigid blade is given.

6. Conclusions and Perspectives

SOFIA has been applied to compute blade deformations during BVI and their impact on the pressure distribution about the rotor-blade. For the prediction of the three-dimensional, compressible (transonic) flow a modification of the well-known INFLEX code is used. The structural analysis is done using ODISA - a code based on TIMOSHENKO-beam theory. An aeroelastic analysis of a rotor-blade undergoing a blade-vortex interaction has been performed to demonstrate the feasibility of SOFIA to treat this highly complex phenomenon. The computations are promising and show that the full coupling of CFD and structural analysis can indeed be used to make a significant contribution to the understanding of vibratory loads and acoustics. Furthermore SOFIA offers the opportunity to study the impact of control movements from active control devices on the rotor blade's flowfield.

7. Acknowledgements

This work was partially supported by the Deutsche Forschungsgemeinschaft. We would like to thank Dr. A. Brenneis and Dr. A. Eberle from the DASA for the provision of the computer code INFLEX. Computations were performed using the facilities of the Rechenzentrum der RWTH Aachen.

8. Literature

1. G.E.A. Meier and R. Timm, Unsteady Vortex Airfoil Interaction, AGARD CP-386, 1985, 16.1-16.10

2. F.X., Caradonna, R.C. Strawn and J.O. Bridgeman, An Experimental and Computational Study of Rotor-Vortex Interactions, 14th European Rotorcraft Forum, 1988

3. D. Bershader, Shock Tube Studies of Vortex Structure and Behaviour, in: H. Grönig (Ed.), Proc. of the 16th Int. Sym. on Shock Tubes and Waves, Aachen, July 1987, Weinheim, VCH, 1988

4. M.H. Horner, E. Saliveros and R.A. Mc. D. Galbraith, An Experimental Investigation of the Oblique Blade-Vortex Interaction, 17th European Rotorcraft and Lift Aircraft Forum, Berlin, Germany, Sept. 1991

5. H.E. Jones and F.X. Caradonna, Full-Potential Modelling of Blade-Vortex Interactions, 12th European Rotorcraft Forum, Paper No. 27, 1986

6. G.R. Srinivasan, W.J. McCroskey and J.D. Baeder, Aerodynamics of Two-Dimensional Blade-Vortex Interaction, AIAA-Journal, Vol. 24, No. 10, Oct. 1986

7. J. Ballmann and C. S. Kocaaydin, Some Aerodynamic Mechanisms of Impulsive Noise during Blade-Vortex-Interaction, 16th European Rotorcraft Forum,1990

8. S. Körber and J. Ballmann, Aerodynamik und Aeroakustik bei Wirbel-Profil-Wechselwirkungen, 8. DGLR Fachsymposium, Strömungen mit Ablösungen, 1992

9. W.R. Splettstoesser, K.-J. Schultz, R. Kube, T.F. Brooks, E.R. Booth, G. Niesl and O. Streby, BVI Impulsive Noise Reduction By Higher Harmonic Pitch Control: Results Of A Scaled Model Rotor Experiment In The DNW, 17th European Rotorcraft Forum, 1991

10. P. Richter and H.D. Elsbrechter, Design and First Tests of Individual Blade Control Actuators , 16th European Rotorcraft Forum, 1990

11. A. Brenneis and A. Eberle, Application of an Implicit Relaxation Method Solving the Euler Equations for Time-Accurate Unsteady Problems, Journal of Fluids Engineering, Vol. 112, Dec 1990, pp 510-520

12. A. Brenneis and A. Eberle, Evaluation of an Implicit Euler Code Against Two and Three-Dimensional Standard Configurations, in: AGARD CP-507: Transonic Unsteady Aerodynamics and Aeroelasticity, Paper No. 10, March 1992

13. A. Eberle, 3D Euler Calculations Using Characteristic Flux Extrapolation, AIAA Paper 85-0119, 1985

14. S.R. Chakravarthy, Relaxation Methods for Unfactored Implicit Upwind Schemes, AIAA Paper 84-0165, 1984

15. W. Schwarz, Elliptic System for Three-Dimensional Configurations Using Poisson Equations, Numerical Grid Generation in Computational Fluid Dynamics, 1st. ed., Pineridge Press, 1986, pp 341-352

16. H.D. Lauermann and J. Ballmann, Instationäre Verformungen elastischer Rotorblätter, ZAMM 70, 1990

17. D. Nellessen, S. Schlechtriem and J. Ballmann, Numerical Simulation of Flutter Using the Euler Equations, Notes on Numerical Fluid Mechanics, 1992

18. K. Ramachandran, S. Schlechtriem, F.X. Caradonna, J. Steinhoff, The Application of Vorticity Embedding to the Computation of Advancing Rotor Flows, presented at the 49th AHS Annual Forum, St. Louis, MO, 1993

19. S. Schlechtriem, K. Ramachandran, F.X. Caradonna, J. Steinhoff: " Free-Wake Computation of Helicopter Rotor Flowfields in Forward Flight ", AIAA - 93 - 3079, 1993

20. F. John: Partial Differential Equations, Springer, Berlin, 1990

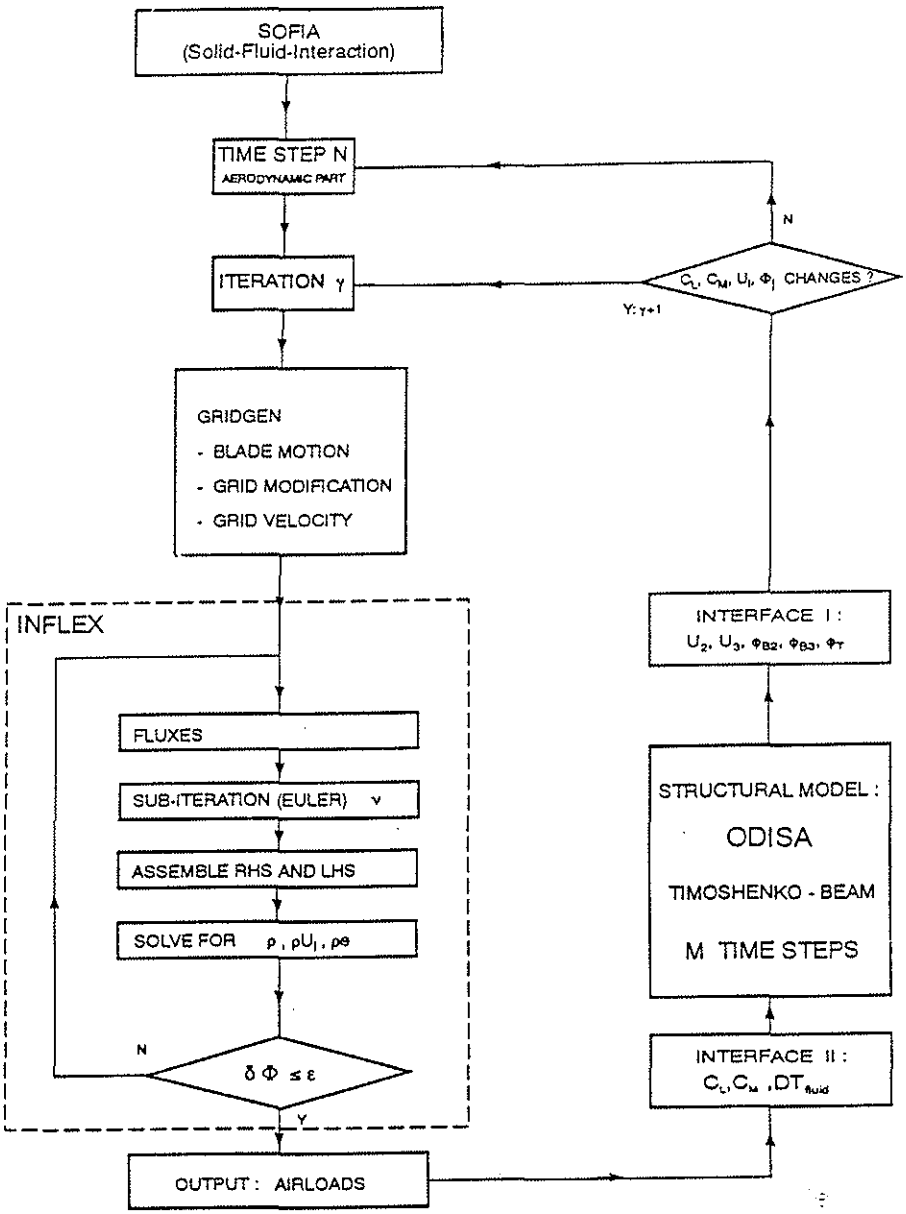

Figure 1: Schematic of the SOFIA solution procedure

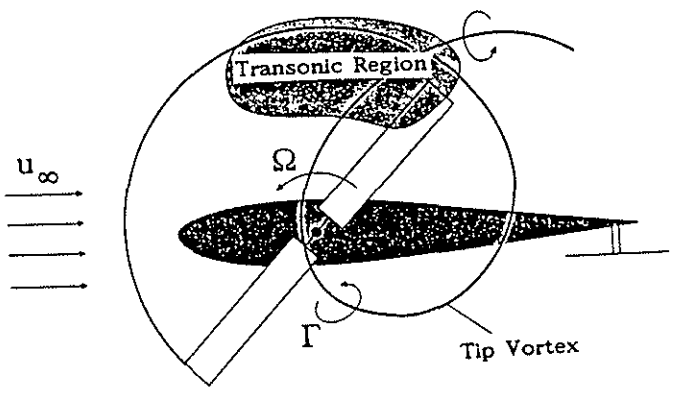

Figure 2: Helicopter in forward flight

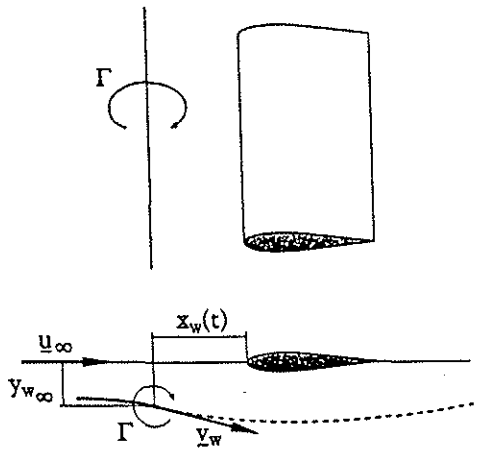

Figure 3: Two-dimensional idealization of a blade-vortex-interaction

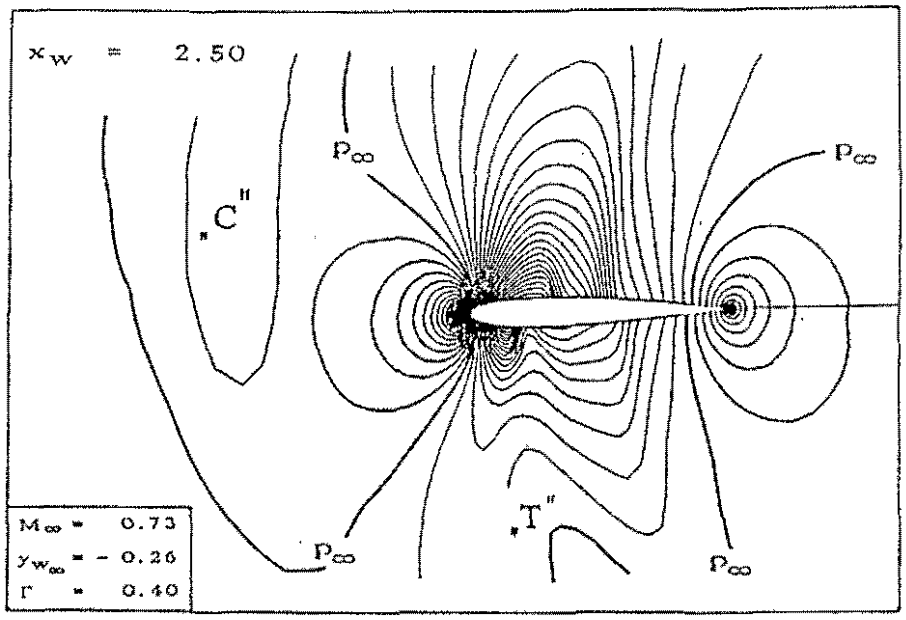

Figure 4: Pressure contours during a blade-vortex-interaction ("C" = compressibility wave, "T" = transonic wave)

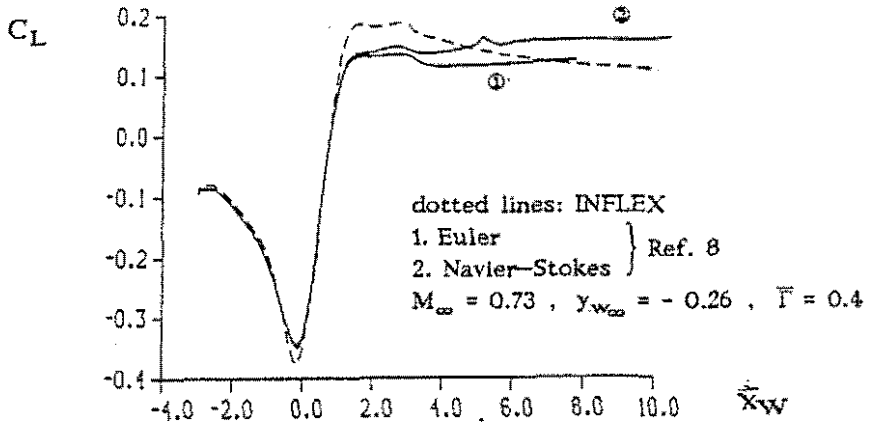

Figure 5: Comparison of the lift coefficient for a blade–vortex-interaction

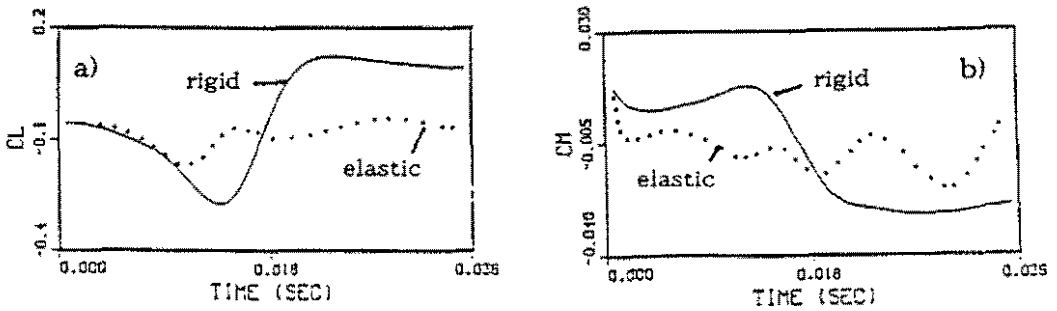

Figure 6: Airloads during BVI; elastic blade versus rigid blade (NACA 0012 , M_∞ = 0.81 , y_{w_∞} = - 0.3 , $\bar{\Gamma}$ = 0.4 $\bar{\omega}_1$ = 1.01 , $\bar{\omega}_2$ = 1.22 , ξ_{3D} = 0.25c , ξ_{3C} = 0.35c)

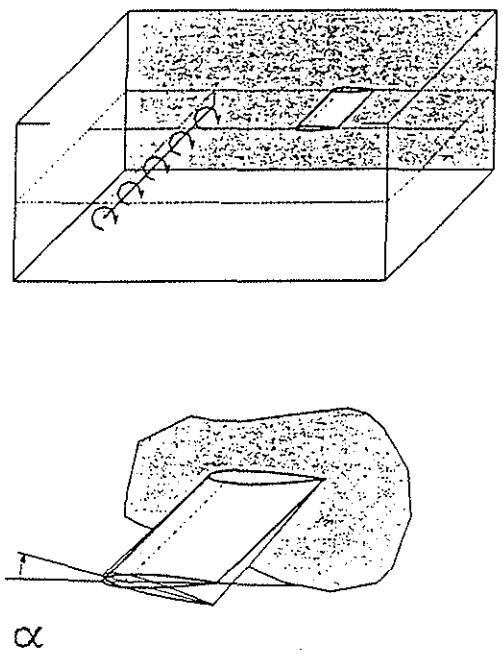

Figure 7: Interaction of a line vortex with a torsionally flexible blade

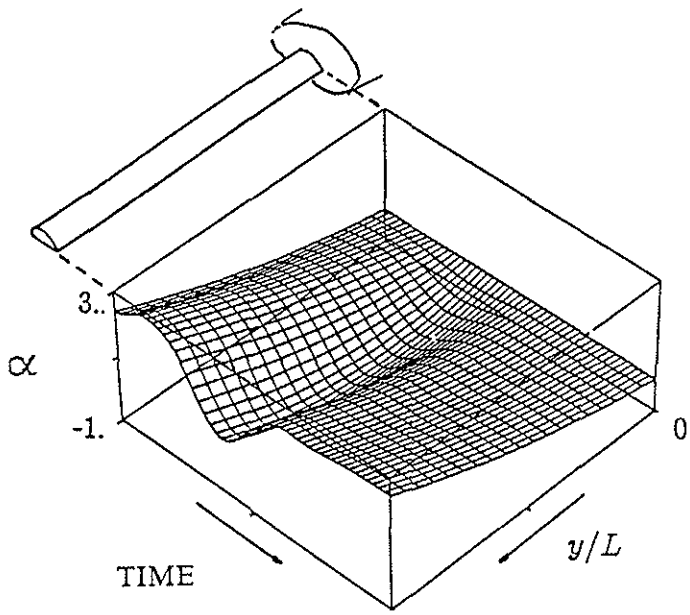

Figure 8: Angle of attack versus time

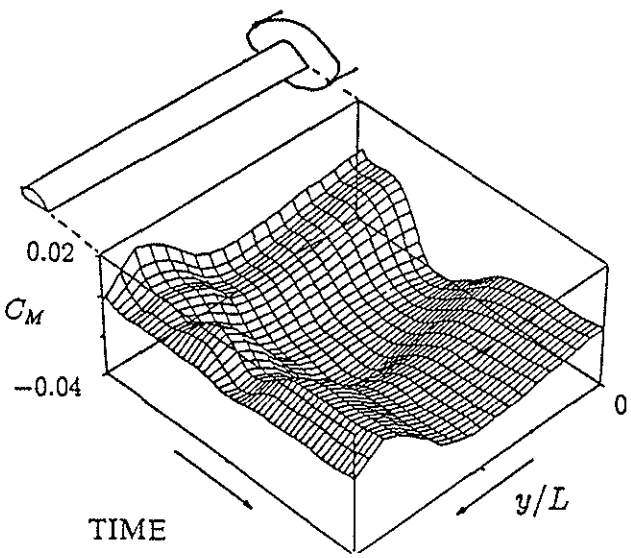

Figure 9: Computed airloads for a torsionally flexible blade

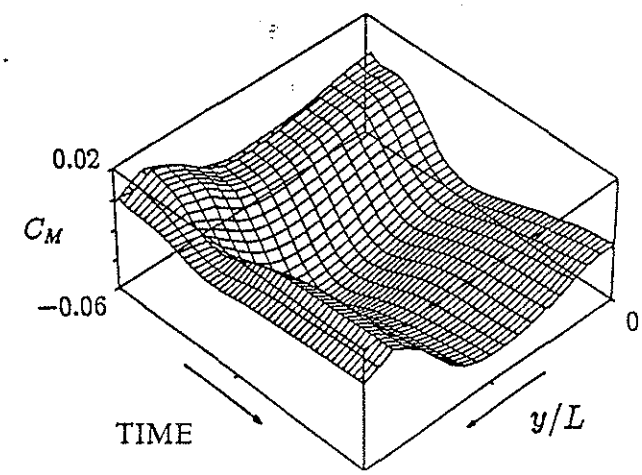

Figure 10: Computed airloads for a rigid blade